Monthly Notices
of the
ROYAL ASTRONOMICAL SOCIETY

MNRAS **471,** 3043–3050 (2017) doi:10.1093/mnras/stx1752

Anisoplanatic error evaluation and wide-field adaptive optics performance at Dome C, Antarctica

M. Carbillet,[1]★† É. Aristidi,[1] C. Giordano[2] and J. Vernin[1]

[1] *Université Côte d'Azur, Observatoire de la Côte d'Azur, CNRS, Laboratoire Lagrange, France*
[2] *INAF–Osservatorio Astrofisico di Arcetri, Largo Enrico Fermi 5, I-50125 Firenze, Italy*

Accepted 2017 July 11. Received 2017 May 25; in original form 2016 March 3

ABSTRACT

The aim of this paper is twofold: (i) to deduce the most representative C_N^2 profile(s) for Dome C (DC), Antarctica, from the latest measurements, and (ii) to evaluate the performance of a wide-field adaptive optics (AO) system equipping a 2–3 m telescope. Two models of the C_N^2 profile, corresponding to the bimodal distribution of seeing (a poor seeing mode and a good seeing mode), are composed from both Single Star Scidar data and balloon radio soundings. The anisoplanatic error is first evaluated for a standard AO system from Monte Carlo simulations. DC is shown to outperform Mauna Kea for both seeing modes. A simple ground-layer AO (GLAO) system is then considered. This provides an anisoplanatic error of less than 150 nm over a field of 30 arcmin for the good seeing mode, corresponding to a basic performance Strehl ratio (considering also the fitting and the servo-lag errors) of more than ∼80 per cent in K and ∼50 per cent in J. The poor seeing model shows performance comparable to the Mauna Kea model. We also studied the influence of telescope elevation, showing that a telescope at 40 m would perform, in the poor seeing mode, like a telescope observing 8 m above the ground in the good seeing mode. Finally, we show that while tip-tilt-only correction permits high levels of correction in the good seeing mode at 40 m, it is not as efficient as the GLAO system, even at an altitude of 8 m, and it is not sufficient for high levels of correction for poor seeing, even at a height of 40 m.

Key words: atmospheric effects – instrumentation: adaptive optics – methods: data analysis – methods: numerical.

1 INTRODUCTION

Since the beginning of the characterization campaigns at Dome C (DC), Antarctica (Aristidi et al. 2003), the site has been known as peculiar because of its very thin but very turbulent surface layer (SL) (Lawrence et al. 2004; Agabi et al. 2006; Trinquet et al. 2008; Lascaux, Masciadri & Hagelin 2011), and its very dry atmosphere. Aristidi et al. (2009) showed that, during summer (corresponding to daytime at DC), the seeing has a median value of $\varepsilon_0 = 0.57$ arcsec, and that this median value would increase to more than 1 arcsec in winter (night-time at DC). However, they also showed that the seeing histogram actually displays a bimodal distribution with a sharp good seeing peak and a broader poor seeing one. Giordano et al. (2012), using their Single Star Scidar (SSS) (Vernin et al. 2009), found also that during winter, the median value of the seeing is $\varepsilon_0 = 1$ arcsec and they confirmed its bimodal distribution. They also emphasize the temporal stability of the atmosphere, which was also reported by Fossat et al. (2010).

This particular structure of the turbulent atmosphere at DC (a very thin but strong turbulent SL), together with the confirmed bimodal distribution of seeing, raises the question of the relevance and efficiency of a wide-field adaptive optics (AO) system equipping a telescope of reasonable size operating in the near-infrared at DC. Indeed, the large coherence time should allow us to reduce the delay error. The small seeing value allows us to easily and benefit from a rather good correction. The large isoplanatic angle will allow us to reduce the anisoplanatic error and enlarge the sky coverage, and it will give us very wide fields of correction. However, as underlined by Andersen et al. (2006) in the context of wide-field AO performance evaluation, the thickness of the boundary layer is of fundamental importance for the size of the compensated field, the uniformity of the point-spread function, and the ratio of aberrations in the boundary layers to those in the free atmosphere for image quality.

The present study pursues the same line as the work initiated in Lawrence et al. (2008), Travouillon et al. (2009) and Carbillet et al. (2010a). It is based on an analysis of the latest seeing measurements

★ E-mail: marcel.carbillet@oca.eu
† Address: Laboratoire Lagrange, Bât. Fizeau, Parc Valrose, 06100 Nice, France.

and focuses on the bimodal characteristics of the DC turbulent atmosphere. The framework is the same as for the telescope project PILOT (Saunders et al. 2008a,b), and similar projects (Le Roux et al. 2008; Moretto et al. 2012; Abe et al. 2013). Both a single-reference AO system (hereafter called standard AO) and a ground-layer AO (GLAO) (Shmalhausen & Yaitskova 2000; Rigaut 2003; Tokovinin 2004) system are simulated to take full advantage of the peculiarity of the DC atmosphere. GLAO is usually considered only to improve the concentration of the point-spread function (the so-called seeing enhancement), leaving the goal of diffraction-limited imaging to standard AO for narrow fields, or to more refined (and complex) multiconjugate AO for wide fields. Here we consider using a simple GLAO system for (nearly) diffraction-limited imaging for a very wide field of view (30 arcmin).

The bimodal structure of the turbulence above DC is discussed in Section 2, while the simulation results of the AO systems considered for a 2.4-m optical telescope are presented in Section 3, including a discussion on the height of the telescope and the possibility of using only tip–tilt correction. Conclusion are then given in Section 4.

2 OPTICAL TURBULENCE PROFILES

Winter DC site-testing campaigns have been conducted since the opening of the Franco-Italian Concordia station in 2005. A number of instruments have been deployed to monitor the turbulence. A differential image motion monitor (DIMM) located 8 m above the snow surface provides a seeing value every 2 min. Statistical analysis of these data by Aristidi et al. (2009) shows that, during winter, the seeing histogram displays a bimodal distribution with a sharp peak centred at ∼0.4 arcsec (corresponding to 16 per cent of the total seeing values at 8 m above ground level) and a broader peak of poor seeing around 1.7 arcsec.

In 2006, the installation of the SSS allowed us to monitor continuously the vertical profiles of the refractive index structure constant C_N^2 and the wind speed from March to September (hence, corresponding to winter, i.e. night-time at DC). These profiles sample the atmosphere in 29 layers, placed between 0 and ∼25 km above ground level. The lowest measured layer, from altitudes 0 to 500 m, is divided into four sub-layers to account for rapid variations of C_N^2 near the surface. From these data, Giordano et al. (2012) showed that the seeing distribution measured by the SSS has the same bimodal shape. This bimodal distribution may come from the SL, which has a general thickness of about 30 m and has most of the turbulent energy (Trinquet et al. 2008). It sometimes become thinner and the instruments are then situated above it, giving access to free atmosphere seeing ($\varepsilon_0 \simeq 0.4$ arcsec), 16 per cent of the time at 8-m altitude and 50 per cent of the time at 20-m altitude (Aristidi et al. 2013). From this peculiar aspect comes the interest in studying the possibility of installing an AO system for wide-field near-infrared, possibly diffraction-limited, imaging.

The principle of our analysis is the following. For each SSS profile obtained during winter 2006, the seeing is computed by numerical integration (Giordano et al. 2012). We then apply a threshold of 0.6 arcsec to discriminate between the poor seeing mode and the good seeing mode. This value of 0.6 arcsec was chosen by considering the SSS seeing histogram, presented in fig. 4 of Giordano et al. (2012), which shows a two-bump structure with a local minimum at 0.6 arcsec between the bumps (i.e. modes).

We obtained two mean vertical distributions for C_N^2 (Fig. 1, asterisks). The good seeing profile has a resulting seeing of 0.46 arcsec at 500 nm (corresponding to a Fried parameter value r_0 of 22.0 cm), which is quite close to the value found by Aristidi et al. (2009) (∼0.4 arcsec), and a turbulence evolution time τ_0 of 9.02 ms. The deduced poor seeing profile gives a resulting seeing of 1.25 arcsec (corresponding to $r_0 = 8.08$ cm) and $\tau_0 \simeq 2.86$ ms. This seeing value is significantly more optimistic that what was measured by Aristidi et al. (2009) (∼1.7 arcsec). It could be inferred that this is due to a bias with the SSS measurements, which was commented on in Giordano et al. (2012). Because of its small pupil diameter of 40 cm, SSS tends to underestimate the value of C_N^2 when the wind speed is too high. As can be seen in Fig. 1, this is critical inside the SL when the turbulence is strong (poor seeing mode) and results in a large difference of two orders of magnitude between SSS values and balloon-borne radio sounding performed during winter 2005 (Trinquet et al. 2008).

Hence, although SSS measurements benefit from the unprecedented statistics, we decided to consider the profiles measured by radio sounding as an alternative to these SSS profiles. We selected a subset of 29 profiles corresponding to $\varepsilon_0 > 0.6$ arcsec, forming our balloon-based poor seeing subset.The remaining seven available profiles constitute our good seeing balloon-based subset (see the average result in Fig. 1, continuous blue plots). However, the small number of balloon measurements do not provide good statistical significance for the mean values of C_N^2, especially at high altitudes. In winter, balloons tear in the cold air during their ascent, and the maximum altitude reached is of the order of 12–15 km. Hence, only one balloon reached an altitude of 18 km in the subset corresponding to the good seeing mode.

Since our primary goal here is to deduce the most significant profile for each of the two seeing modes, we decided to combine the SSS average profiles above 500 m with the balloon-based average profiles below 500 m. Another advantage of this choice is that it allows us to fit better the modelling recommendations formulated by Tokovinin (2004) (see also Lai et al. 2010) for GLAO systems, which translate here into modelizing with a good altitude resolution the turbulent atmosphere below ∼500 m, if the goal is to achieve image quality up to the diffraction limit of the telescope.

The resulting profiles are characterized by a seeing value of 0.53 ± 0.15 arcsec, corresponding to $r_0 = 18.9$ cm, an isoplanatic angle $\theta_0 = 6.5$ arcsec and a coherence time $\tau_0 = 8.41$ ms, for our composite good seeing model. For our composite poor seeing model, the seeing value is 1.9 ± 0.6 arcsec, corresponding to $r_0 = 5.35$ cm, $\theta_0 = 5$ arcsec and $\tau_0 = 1.53$ ms. This composite choice (see Section 3 and Table 1 for more details) globally better fits the results of DIMM monitoring presented in Aristidi et al. (2009), with seeing values of 0.4 ± 0.13 arcsec and 1.7 ± 0.5 arcsec for the good seeing mode and the poor seeing mode, respectively. Note that our good seeing model also matches the measurements used by Lawrence et al. (2004) in their fundamental *Nature* paper in terms of τ_0 and θ_0, which were found to be, respectively, 7.9 ms (8.4 ms in our case) and 5.7 arcsec (6.5 arcsec in our case).

3 ADAPTIVE OPTICS MODELLING AND RESULTS

To reduce memory usage and make the AO numerical simulations possible, we stacked the measured layers and sampled the atmosphere with a limited number of layers, resulting in 10 layers for both our DC models (see Table 1), imposing a minimum of ∼1 per cent for each contribution to the total profile for the weaker layers, and a vertical sampling as low as 8 m for the stronger layers.

This results in, for our composite good seeing model, seven low altitude layers deduced from the balloon measurements (with different thicknesses, from 8 m for the four lowest layers to 300 m for

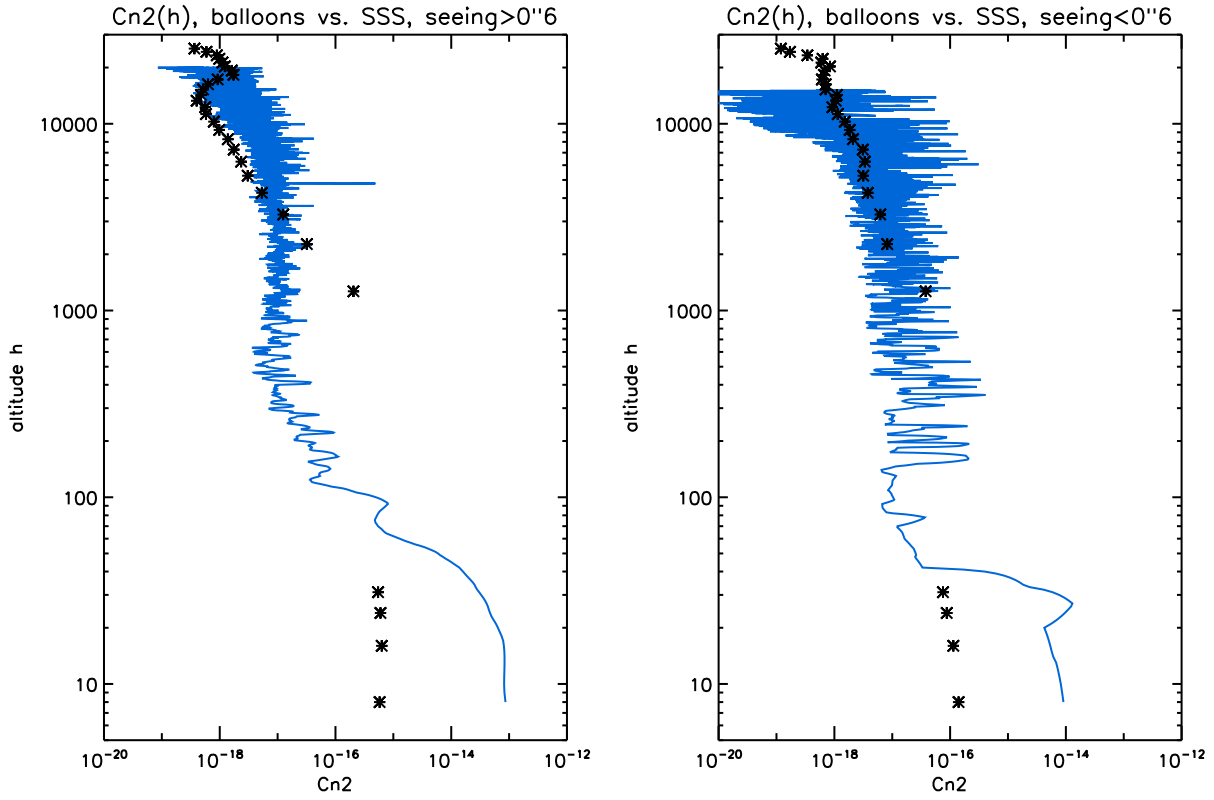

Figure 1. Comparison between the vertical profiles of C_N^2 for SSS and the balloon for the two seeing modes (poor, $\varepsilon_0 > 0.6$ arcsec, to the left, and good, $\varepsilon_0 < 0.6$ arcsec, to the right). The blue continuous profiles correspond to the balloon measurements, while the asterisks correspond to the SSS measurements. Note that the lowest four SSS measurementss are for the four sub-layers within the boundary layer (see text). Note also that DC is 3233 m above sea level. The altitude h given here is above ground level.

Table 1. Percentage of $C_N^2 dh$ (above telescope level, ATL, which is assumed here for DC to be 8 m above ground level, and hence 3241 m above sea level) for each layer of the DC profile models deduced, and associated turbulence parameters used in the following simulations (with the usual reference wavelength of 500 nm), are given in the first four columns. The same quantities for the median profile of the MK site used in the following for comparison are given in the last two columns. The outer scale of turbulence $\mathcal{L}_0$ for DC is from Ziad et al. (2013).

Dome C good seeing		Dome C poor seeing		Mauna Kea	
Altitude ATL [m]	DC, $\varepsilon_0 < 0.6$ arcsec [per cent of $C_N^2 dh$]	Altitude ATL [m]	DC, $\varepsilon_0 > 0.6$ arcsec [per cent of $C_N^2 dh$]	Altitude ATL [m]	MK median profile [per cent of $C_N^2 dh$]
3.8	24.7	4.1	33.7	0	39.370
12.4	18.6	11.7	26.8		
19.7	33.2	19.7	15.8	15	15.433
26.8	5.8	27.7	9.1		
		35.5	4.8	37	9.291
		43.4	2.0		
		61.8	1.4		
100.1	1.3				
169.5	1.6	174.6	1.0	197	3.465
236.6	1.3			357	0.945
				804	7.087
1259.0	6.0	1259.0	4.0		
3080.5	2.9			3171	6.457
		7843.2	1.4	7307	10.394
11107.8	4.6			14636	7.558
r_0 [cm]	18.9	r_0 [cm]	5.35	r_0 [cm]	12.8
$\mathcal{L}_0$ [m]	7.4	$\mathcal{L}_0$ [m]	7.4	$\mathcal{L}_0$ [m]	25.0

the last one), followed by the first 1-km thick layer above measured by SSS, and then two thicker layers resulting from the stacking of the following layers measured by SSS. Our composite poor seeing model results in eight low altitude layers deduced from the balloon measurements (with thicknesses from 8 m for the six lowest layers to 410 m for the last one), followed by two layers from the SSS (the first 1-km thick layer above measured by SSS, and then one layer resulting from the stacking of the rest of the layers measured). Note that the equivalent altitude of each layer presented in Table 1 has been recalculated considering the weight of the local C_N^2 profile.

For comparison, a Mauna Kea (MK) model was also deduced from Chun et al. (2014), but excluding their dome contribution. The MK layer decomposition is shown, together with the DC ones, in Table 1 (and it corresponds to a seeing value of 0.79 arcsec).

3.1 Dimensioning and numerical modelling

Regarding the dimensioning of the system, let us first remark that an AO system working in band J (1.25 μm) would have a Fried parameter r_0 of ∼16 cm within our poor seeing model. This corresponds, for a reasonable Strehl ratio (Strehl 1902) in that band, to an inter-actuator distance equal to that value. On a telescope of diameter $D = 2.4$ m, this corresponds to 15 × 15 subapertures, and then 16 × 16 actuators in the simplified Fried configuration (Fried 1977),[1] i.e. the number of Zernike modes measured and corrected is

$$\frac{(n+1)(n+2)}{2} - 1 = 135$$

(with $n = 15$ and piston being excluded). From the well-known Noll formula (Noll 1976) for Zernike–Kolmogorov residual errors, it can be easily deduced that the equivalent fitting error is

$$\sigma_{\rm fit} \simeq \frac{\lambda}{2\pi} k_{\rm fit} \left(\frac{D}{r_0(\lambda)} \right)^{\frac{5}{6}}$$

with

$$k_{\rm fit} \simeq \sqrt{0.2944} \left(\frac{(n+1)(n+2)}{2} - 1 \right)^{-\sqrt{3}/4} \simeq 0.0649,$$

and hence, ∼43 nm rms for our good seeing model, ∼123 nm rms for our poor seeing model and ∼59 nm for the MK model.

The servo-lag error is given by (Sandler et al. 1994):

$$\sigma_{\Delta t} = \frac{\lambda}{2\pi} \left(\frac{\Delta t}{\tau_0(\lambda)} \right)^{\frac{5}{6}}, \quad (1)$$

resulting, e.g. for a delay time of 2 ms, in ∼24 nm for our good seeing model, ∼99 nm for our poor seeing model and ∼67 nm for the MK model (the τ_0 value for the latter is 2.45 ms; Ziad et al. 2012).

If one considers the whole error budget of an AO system, one would additionally have to consider at least the error due to the wavefront sensor (including both aliasing and measurement errors), and the anisoplanatic error. Other more specific errors may also be considered when building up an actual system, but their evaluation is beyond the scope of this paper. The aliasing error can here be reasonably neglected initially, also because it strongly depends on the kind of wavefront sensor considered – Shack–Hartmann, pyramid, curvature, etc. The measurement error depends on the guide star (GS) magnitude: it is related to a much more classical study of the performance of an AO system with respect to the sensing magnitude.

Instead, we consider in the following that we are in the bright end of such a classical AO performance study (high light level regime). Thus, we consider a basic performance value, where we focus on the two basic on-axis errors due to the turbulent atmosphere, and on the behaviour of a suitable wide-field AO system with respect to the wideness of the corrected field. We end up studying what we call the basic performance of both a single-reference AO system and a multiple-reference GLAO system (assuming that both $\sigma_{\rm fit}$ and $\sigma_{\Delta t}$ remain unchanged for both cases – see e.g. Stoesz et al. 2004), as a function of the off-axis angle θ. Moreover, we make use of the Maréchal approximation (Maréchal 1947) for the resulting Strehl ratio at a given wavelength λ, hereafter denoted by S^λ. Note that, properly speaking, the Maréchal approximation used here actually leads to the coherent energy (Rousset, Madec & Rabaud 1991), which, for sufficiently decent corrections ($S^\lambda > 0.1$), is effectively equivalent to the Strehl ratio (Fusco et al. 2004).[2] The metric used to qualify the systems we study is then:[3]

$$\sigma^2_{\rm basic\ perf}(\theta) = \sigma^2_{\rm fit} + \sigma^2_{\Delta t} + \sigma^2_{\rm aniso}(\theta)$$

$$\Rightarrow S^\lambda_{\rm basic\ perf}(\theta) = S^\lambda_{\rm fit}\, S^\lambda_{\Delta t}\, S^\lambda_{\rm aniso}(\theta). \quad (2)$$

We first compute the anisoplanatic error $\sigma_{\rm aniso}(\theta)$ for the standard AO case for an off-axis angle θ up to 4 arcmin (i.e. a field of correction of 8 arcmin). We then deduce from it the Strehl ratio corresponding to this anisoplanatic error (assuming the Maréchal approximation). Finally, the resulting basic performance Strehl ratio of equation (2) is computed for band J (1.25 μm) and band K (2.2 μm), for a field of correction of 30 arcmin and for a suitable GLAO configuration.

This has been done by numerically modelling the turbulent atmosphere (Carbillet & Riccardi 2010) implemented within the IDL-based Software Package CAOS (Carbillet et al. 2005, 2016), itself developed within the homonymic CAOS Problem-Solving Environment (Carbillet et al. 2004, 2010b). Spatial sampling for the incoming wavefronts was 2.5 cm px^{-1}, resulting in wavefronts/layers up to 5206 × 5206 px (i.e. 130.15 × 130.15 m^2) for the highest layer. A typical computing time for each GLAO case presented in the following was ∼5 d on four cores of a computing machine based on 2.3-GHz AMD Opteron dual cores.

3.2 Standard AO performance

The anisoplanatic error is computed in terms of the average residual rms error over the pupil resulting from the difference between on-axis and off-axis simulated wavefronts, as a function of θ. This rms is then averaged over 1000 independent realizations of atmospheric turbulence, as modelled in Table 1, by considering a von Kármán model of turbulence (Voitsekhovich 1995) and adding subharmonics when necessary (Carbillet & Riccardi 2010).

First, Fig. 2 shows that, despite the well-known excellence of the MK site with respect to atmospheric turbulence conditions, the median MK profile is outperformed by both our DC profile models

[1] The actuators are placed conjugate to the corners of the wavefront sensor subapertures, in a square geometry.

[2] Otherwise the coherent energy is strictly less than the Strehl ratio.

[3] Note that we also make the classical assumption that post-AO errors are uncorrelated, which can, in particular, be untrue for servo-lag and anisoplanatism errors, since, for example, a space shift of the wavefront due to the relative position of the GS and the observed object can be compensated for by an opposite time shift due to wind (Jolissaint 2010).

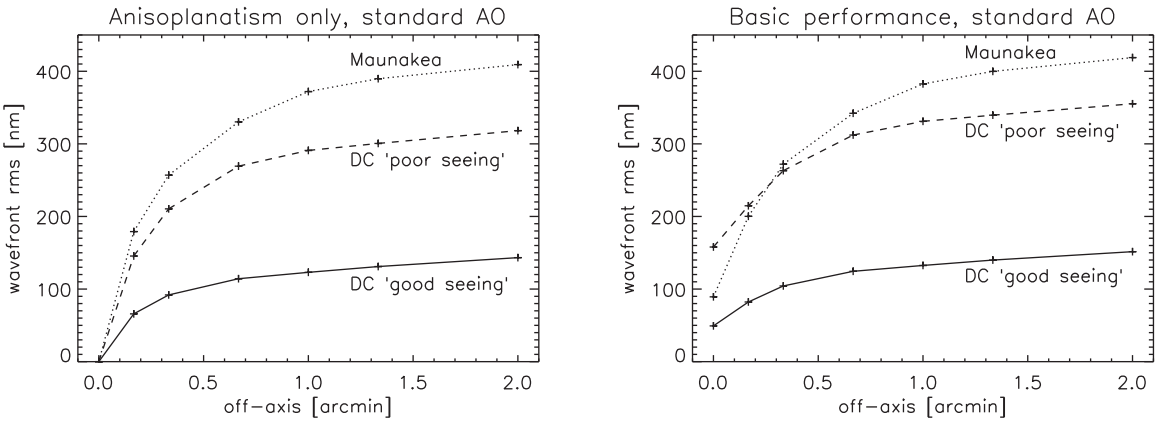

Figure 2. Standard AO case. Right: Wavefront anisoplanatic rms error for both the DC seeing models (good: continuous line and poor: dashed line), and the median MK profile (dotted line). Left: Basic performance rms error.

regarding the anisoplanatic error (in terms of wavefront rms; left plot), because of the different structure of the turbulent atmospheres.

As a consequence, Fig. 2 also shows that our DC good seeing model leads to better basic performance than the MK model – this is also due to better $\sigma_{\rm fit}$ and $\sigma_{\Delta t}$ values for the DC good seeing model. For the same reason, MK has a better on-axis correction than the DC poor seeing model, but DC becomes superior for off-axis angles greater than 20–30 arcsec, when the sensitivity to the anisoplanatic error begins to dominate over the sensitivity to the fitting error and temporal error. This clearly confirms the interest in studying in detail the wide-field performance of a GLAO system at DC, for both our good seeing and poor seeing models.

3.3 Ground-layer AO performance

For the GLAO case, and after a few numerical simulations involving three or four GSs, we found that a simple asterism configuration of one GS at the centre of the field and three GSs arranged regularly on a circle of 15 arcmin diameter actually permits us to reach an almost constant Strehl ratio loss due to anisoplanatism only of less than ∼50 per cent in the J and K bands over the whole 30 arcmin field (actually as low as ∼10–15 per cent in band K and less than ∼25–45 per cent in band J, see Fig. 3, middle left and bottom left plots). Note that the wavefront rms anisoplanatic error (Fig. 3, top left plot) is actually identical between the MK profile and the DC poor seeing profile only at the very border of the chosen 30 arcmin field. Note also that the significant decrease of the wavefront rms error for $\theta = 0$ and $\theta = 7.5$ arcmin occurs where one of the GSs lies in a line across the field. The two other GSs are at $\theta = -7.5$ arcmin, but with position angles of 120 and 240 deg, respectively.

When considering our so-called basic performance (Fig. 3, right plots), note that, while the results for DC poor seeing remain close to those for MK (the anisoplanatic error is slightly better but the fitting error and the temporal error are clearly worse), which does not permit diffraction-limited images but rather classical GLAO seeing enhancement, in a similar manner as for MK, DC good seeing gives Strehl ratios better than ∼80 per cent in band K and ∼50 per cent in band J. Hence, this allow us to consider diffraction-limited near-infrared imaging over the whole 30 arcmin field, with the help of a rather modest wide-field AO system (15 × 15 subapertures and four GSs).

3.4 Telescope altitude and tip–tilt-only correction

Raising the altitude of the telescope intrinsically lowers the number of turbulent layers through which starlight propagates. As a consequence, the resulting r_0 and τ_0 values of the remaining turbulent atmosphere become larger. For poor seeing, r_0 goes from 5.35 cm with $h_{\rm tel} = 8$ m, to 17 cm with $h_{\rm tel} = 40$ m, and τ_0 from 1.53 ms to 3.4 ms.

As can be clearly seen from Fig. 4 (left plot) and Table 2, this last case (poor seeing for $h_{\rm tel} = 40$ m) also leads to an anisoplanatic error very close to that of good seeing for $h_{\rm tel} = 8$ m (139 ± 30 nm and 133 ± 32 nm, respectively).[4] Hence, the anisoplanatic error induced by the poor seeing model of turbulence can indeed be compensated for by raising the telescope to an altitude of 40 m. In contrast, for good seeing, raising the altitude of the telescope does not provide a significant enhancement of the anisoplanatic error (it goes from 133 ± 32 nm for $h_{\rm tel} = 8$ m to 126 ± 33 nm for $h_{\rm tel} = 40$ m).

The compensation due to raising the telescope from 8 to 40 m for poor seeing also happens for the fitting error $\sigma_{\rm fit}$, which goes from 123 to 47 nm, a value very close to that for good seeing with $h_{\rm tel} = 8$ m (43 nm). This is, however, not the case for $\sigma_{\Delta t}$, which goes from 99 to 51 nm. This remains significantly larger than for good seeing with $h_{\rm tel} = 8$ m (24 nm). Nevertheless, since the last error does not apply here, it can be stated that considering poor seeing with $h_{\rm tel} = 40$ m appears equivalent to considering good seeing with $h_{\rm tel} = 8$ m, with a basic performance error over the field of 155 ± 27 nm for poor seeing with $h_{\rm tel} = 40$ m, and of 142 ± 30 nm for good seeing with $h_{\rm tel} = 8$ m.

Finally, note that raising the telescope from 8 to 40 m also reduces $\sigma_{\rm fit}$ and $\sigma_{\Delta t}$ for good seeing, which goes, respectively, from 43 nm to 18 nm, and from 24 nm to 15 nm. However, this leads to a more modest enhancement of the basic performance error over the field, going from 142 ± 30 nm to only 128 ± 32 nm.

In all those cases when the effects of the boundary layer turbulence are substantially eliminated or intrinsically low (poor seeing for $h_{\rm tel} = 40$ m or good seeing for $h_{\rm tel} = 8$ m), we could consider the tip–tilt correction only,[5] as recommended in Saunders et al. (2008b). In fact, for poor seeing, $\sigma_{\rm fit}$ would be dramatically reduced, going

[4] The error bars here are obtained by propagating the rms over the 1000 measurements made of the anisoplanatic error for each off-axis angle. This is not reported in the plots for readability.

[5] Note that here we are considering a tip–tilt sensing based on four GSs, as for the 15 × 15-subaperture system case.

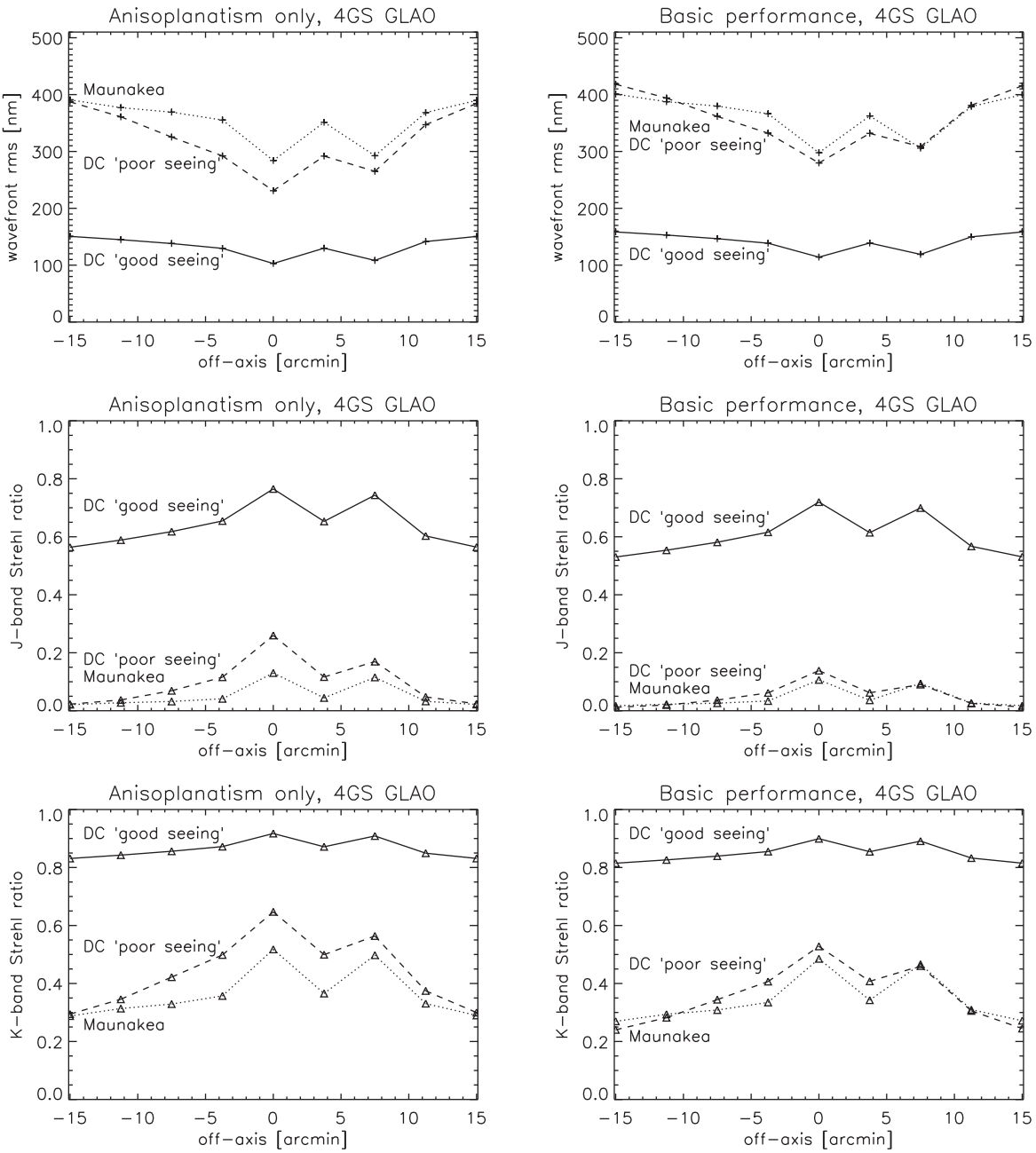

Figure 3. 4-GS GLAO case. Top: Wavefront anisoplanatic rms error for both the DC seeing models (good: continuous line and poor: dashed line), and the median MK profile (dotted line). Middle: Strehl ratios for the *J* and *K* bands due to anisoplanatism only. Bottom: *J* and *K* band basic performance Strehl ratios.

from 762 nm (for a telescope at an altitude of 8 m and tip–tilt correction only) to 291 nm when the telescope is at 40 m ($k_{\rm fit}$ goes from ∼0.0649 to ∼0.402 considering only two modes instead of the 135 allowed by the 15 × 15-subaperture system), but it still remains much higher than the 123 nm (for $h_{\rm tel} = 8$ m) or 47 nm (for $h_{\rm tel} = 40$ m) given by the 15 × 15-subaperture system. On the other hand, it is also true that the anisoplanatic error goes from ∼321 ± 72 nm over the field to ∼139 ± 30 nm, thanks to raising the telescope altitude from 8 to 40 m. Consequently, the basic performance error goes from 358 ± 69 nm for poor seeing with $h_{\rm tel} = 8$ m and the full correction allowed by the 15 × 15 system, to 327 ± 13 nm with $h_{\rm tel} = 40$ m and tip–tilt correction only. In the same manner, the basic performance error goes from 142 ± 30 nm for good seeing with $h_{\rm tel} = 8$ m and the full correction allowed by the 15 × 15 system, to 169 ± 25 nm with $h_{\rm tel} = 40$ m and tip–tilt correction only. Hence, here again there is compensation, but it works the other way: the effect of raising a telescope equipped with tip–tilt-only correction from 8 to 40 m can be roughly compensated for by equipping the telescope with a 15 × 15 system with $h_{\rm tel} = 8$ m, although with a lower uniformity of correction over the field (see Fig. 4, right plot).

Diffraction-limited images in the near-infrared can be attained for good seeing with any telescope altitude and a 15 × 15 GLAO system, or with a simpler tip–tilt-only system but at $h_{\rm tel} = 40$ m. This can also be achieved for poor seeing but with the 15 × 15

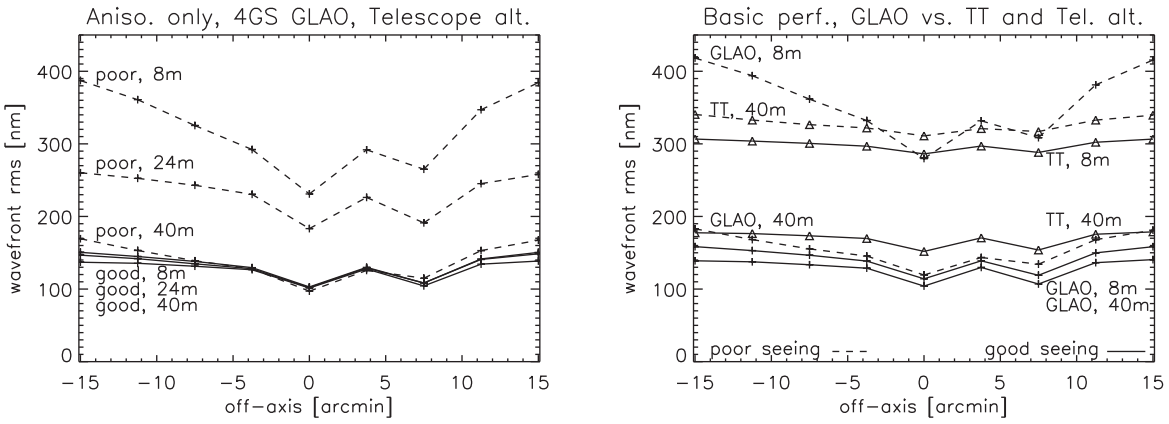

Figure 4. Left: Influence of telescope altitude ($h_{\rm tel}$) on the wavefront anisoplanatic rms error, for the 4-GS GLAO case and for both the DC poor seeing and the good seeing models, as a function of the three cases of $h_{\rm tel}$ examined: 8, 24 and 40 m. Right: GLAO versus the same curves for a GLAO and a tip–tilt (TT) system.

Table 2. Various errors for the two DC atmosphere models and the two cases of $h_{\rm tel}$ discussed in the text.

Error	DC poor seeing		DC good seeing	
[nm]	8 m	40 m	8 m	40 m
$\sigma_{\rm aniso}$	321 ± 72	139 ± 30	133 ± 32	126 ± 33
$\sigma_{\rm fit,15\times15}$	123	47	43	18
$\sigma_{\rm fit,\ tip-tilt}$	762	291	266	112
$\sigma_{\Delta t}$	99	51	24	15
$\sigma_{\rm basic\ perf,15\times15}$	358 ± 69	155 ± 27	142 ± 30	128 ± 32
$\sigma_{\rm basicperf,tip-tilt}$	833 ± 28	327 ± 13	298 ± 14	169 ± 25

GLAO system installed at $h_{\rm tel} = 40$ m. More traditional GLAO correction levels (seeing enhancement) can still be obtained with a tip–tilt system at $h_{\rm tel} = 8$ m for good seeing, but for poor seeing this requires either putting the telescope at an altitude of 40 m or having a 15 × 15 GLAO system.

4 CONCLUSIONS

It is clear from the plots of Section 3.3 that a GLAO system with only four GSs arranged in a field of 15 arcmin installed on a 2.4-m telescope at DC, Antarctica, can give an outstanding and stable wide-field correction over 30 arcmin for our composite good seeing model, leading to a basic performance Strehl ratio of ∼80 per cent in band K and ∼50 per cent in band J. On the other hand, our composite poor seeing model gives less impressive results, being roughly equivalent to the MK model, and hence, it does not deliver the Strehl ratio levels necessary to allow diffraction-limited near-infrared images, but still permits seeing enhancements with a more classical use of a GLAO system with the same level of equipment installed at MK.

However, we also showed that for good seeing, tip–tilt-only correction at $h_{\rm tel} = 40$ m gives excellent correction quality, and even better is a 15 × 15 GLAO system at 8 m. For poor seeing, it is necessary to have both a 15 × 15 GLAO system and $h_{\rm tel} = 40$ m to obtain similar results. Note that the classical GLAO seeing enhancement can still be obtained with tip–tilt-only correction at a height of 8 m for good seeing, and at 40-m or with a 15 × 15 GLAO system for poor seeing.

Compared to previous works, Travouillon et al. (2009) and Carbillet et al. (2010a), the profiles presented and used here are definitely more representative. In fact, those papers were based on a median C_N^2 profile, mixing good and poor seeing modes, which does not reflect real situations. The present results are deduced from two realistic and physically different atmospheric configurations. In addition, the preliminary results detailed in Carbillet et al. (2010a) were computed from a whole evaluation of the final AO error budget, including star-magnitude-dependent errors, while the present results permit us to clearly disentangle each fundamental error. As a consequence, this leads to more readable and usable results for future detailed AO system studies for DC, which will, hence, be able to benefit from our estimation of the anisoplanatic error and the corresponding Strehl ratio.

Finally, note that the good seeing mode is observed only 16 per cent of the time in winter for a telescope located at an elevation of 8 m above the ground. However, this percentage would be higher, as discussed by Travouillon et al. (2009), if the telescope were placed higher. For example, on a 20-m high tower, the telescope would be above the SL for 50 per cent of the time (Aristidi et al. 2013).

ACKNOWLEDGEMENTS

Thanks are due to François-Xavier Schmider and Éric Fossat (Laboratoire Lagrange) for preliminary discussions about this work. Data were collected within the scope of the polar program Institut Paul Émile Victor (IPEV)/AstroConcordia. The authors gratefully acknowledge the polar agencies IPEV and Programma Nazionale di Ricerche in Antartide (PNRA), and the French agency Institut National des Sciences de l'Univers (INSU) for logistical support and funding. We thank also the local DC staff for their assistance.

We also wish to thank the anonymous referee, whose remarks and suggestions allowed us to exploit better the various site testing data available for DC, and hopefully to clarify the presentation of the results obtained.

REFERENCES

Abe L. et al., 2013, Proc. IAU Symp. 288. Kluwer, Dordrecht, p. 243
Agabi A., Aristidi E., Azouit M., Fossat É., Martin F., Sadibekova T., Vernin J., Ziad A., 2006, PASP, 118, 344
Andersen D. R. et al., 2006, PASP, 118, 1574
Aristidi E., Agabi A., Vernin J., Azouit M., Martin F., Ziad A., Fossat E., 2003, A&A, 406, L19
Aristidi É. et al., 2009, A&A, 499, 955
Aristidi É. et al., 2013, Proc. IAU Symp. 288. Kluwer, Dordrecht, p. 300
Carbillet M., Riccardi A., 2010, App. Optics, 49, G47
Carbillet M. et al., 2004, SPIE Proc., 5490, 550
Carbillet M., Vérinaud C., Femenía B., Riccardi A., Fini L., 2005, MNRAS, 356, 1263
Carbillet M., Maire A.-L., Le Roux B., Aristidi É., Giordano C., Pasqueron de Fommervault O., Gautier J., Trinquet H., 2010a, EAS Publ. Series, 40, 157
Carbillet M., Desiderà G., Augier É., La Camera A., Riccardi A., Boccaletti A., Jolissaint L., Ab Kadir D., 2010b, SPIE Proc., 7736, 773644
Carbillet M., La Camera A., Folcher J.-P., Perruchon-Monge U., Adama S., 2016, SPIE Proc. 9909, 9909-31.
Chun M. R. et al., 2014, SPIE Proc., 9148, 91481K
Fossat É., Aristidi É., Agabi A., Bondoux É., Challita Z., Jeanneaux F., Mékarnia D., 2010, A&A, 517, 69
Fried D. L., 1977, J. Opt. Soc. America, 67, 370
Fusco T. et al., 2004, SPIE Proc., 5490, 118
Giordano C., Vernin J., Chadid M., Aristidi É., Agabi A., Trinquet H., 2012, PASP, 124, 494
Jolissaint L., 2010, J. European Opt. Soc., Rapid Publication, 5
Lai O., Chun M. R., Pazder J., Véran J.-P., Jolissaint L., Andersen D., Salmon D., Cuillandre J.-C., 2010, SPIE Proc., 7736, 77361D
Lascaux F., Masciadri E., Hagelin S., 2011, MNRAS, 411, 693
Lawrence J. S., Ashley M. C. B., Tokovinin A., Travouillon T., 2004, Nature, 431, 278
Lawrence J. S., Ashley M. C. B., Storey J. W. S., Jolissaint L., Travouillon T., 2008, PASP, 120, 1119
Le Roux B., Carbillet M., Langlois M., Trinquet H., Burgarella D., Ferrari M., Schmider F.-X., 2008, SPIE Proc., 7015, 70154G
Maréchal A., 1947, Rev. Opt. Théor. Instrum., 26, 257
Moretto G., Epchtein N., Langlois M., Vauglin I., 2012, SPIE Proc., 8444, 84445E
Noll R., 1976, J. Opt. Soc. America, 66, 207
Rigaut F., 2003, ESO Conf. Proc., 58, 421
Rousset G., Madec P. Y., Rabaud D., 1991, ESO Conf. Proc., 39
Sandler D. G., Stahl S., Angel R., Lloyd-Hart M., McCarthy D., 1994, J. Opt. Soc. America A, 11, 925
Saunders W., Gillingham P., McGrath A., Haynes R., Brzeski J., Storey J., Lawrence J., 2008a, SPIE Proc, 7012, 70124F
Saunders W. et al., 2008b, SPIE Proc, 7014, 70144N
Shmalhausen V., Yaitskova N., 2000, SPIE Proc., 4338, 97
Stoesz J. A., Jolissaint L., Véran J.-P., LeDue J., 2004, SPIE Proc., 5490, 713
Strehl K., 1902, Z. Instrumentenkd, 22, 213
Tokovinin A., 2004, PASP, 116, 941
Travouillon T., Jolissaint L., Ashley M. C. B., Lawrence J. S., Storey J. W. V., 2009, PASP, 121, 668
Trinquet H., Agabi A., Vernin J., Azouit M., Aristidi É., Fossat É., 2008, PASP, 120, 203
Vernin J., Chadid M., Aristidi É., Agabi A., Trinquet H., van der Swaelmen M., 2009, A&A, 500, 1271
Voitsekhovich V. V., 1995, J. Opt. Soc. America A, 12, 1346
Ziad A., Blary F., Borgnino J., Dali Ali J., Berdja A., Maire J., Martin F., 2012, J. Opt., 14, 045705
Ziad A. et al., 2013, A&A, 559, L6

This paper has been typeset from a TEX/LATEX file prepared by the author.